JOURNAL OF GUIDANCE, CONTROL, AND DYNAMICS
Vol. 29, No. 1, January–February 2006

Robust Navigation Using the Global Positioning System in the Presence of Spoofing

Yaakov Oshman* and Mark Koifman†
Technion—Israel Institute of Technology, 32000 Haifa, Israel

The conventional approach used for identifying faults in global positioning system (GPS) receivers is based on snapshot algorithms belonging to the class of receiver autonomous integrity monitoring (RAIM) algorithms. A new approach is presented for alleviating the effects of spoofing disturbances in GPS receivers. Based on the interacting multiple model (IMM) estimator, this approach may be used in stand-alone GPS systems and in integrated systems, such as GPS-embedded inertial navigation systems. The IMM-based method not only provides (implicit) detection and identification of the interference, but also an optimal estimate of the state of the system in the presence of this interference. In addition, contrary to the conventional detect, identify, and exclude RAIM approach, the new method's probabilistically weighted estimate is obtained without excluding any satellite from the solution. Numerical simulations are used to demonstrate the superiority of the proposed approach over the conventional RAIM approach in scenarios having unfavorable satellite constellation geometries. The robustness of the new approach is shown for a wide range of spoofing signal types. In addition, the new algorithm is shown to perform adequately with just five satellites, which is below the minimum number of satellites required for RAIM fault identification.

I. Introduction

THE Global Positioning System (GPS) is increasingly used as the main navigation system in various applications (ground, airborne, maritime, civil, and military). This is because of its high performance-to-cost ratio, especially after the cancellation of the selective availability intentional error. The system can be used in stand-alone mode or as part of an integrated system, such as a GPS-embedded inertial navigation system (INS). Nevertheless, because GPS signals can be jammed or interfered with quite easily, this system cannot be relied on for certain critical applications without additional measures that will provide an indication about the integrity state of its output. The system indeed provides the user with basic integrity data as part of the navigation message broadcast from the satellite to the receiver; however, this is not sufficient for certain civilian applications and certainly not for military uses, where unintended or deliberate interference (electronic warfare) by an enemy must be taken into account. For this reason, additional means are needed to monitor the soundness of the system.

The problem addressed in this paper is that of GPS navigation in the presence of spoofing, which is a deliberate transmission of falsified signals, meant to fool a GPS receiver.[1,2] In the present work it is assumed that GPS spoofing can be represented as a deliberate, time-varying bias, introduced in the measurements of one or more of the acquired satellites. The case of signal jamming, manifested as a uniform increase of the measurement noise or a complete blocking of the signals, is not dealt with here. This case is easier to detect and is, usually, handled well by signal conditioning algorithms embedded in GPS receivers or by estimation methods.[3]

In receiver autonomous integrity monitoring (RAIM) algorithms, the receiver itself decides on the integrity of the system, based only on testing the consistency of information arriving from the GPS satellites. Clearly, this approach may be used only in cases where there is redundancy in the acquired data. This approach is especially suitable for applications where the autonomy of the system is a prime factor. The RAIM concept was first proposed by Kalafus in 1987.[4] Two different classes of algorithms have been suggested for the implementation of the RAIM approach. The first is the class of snapshot algorithms. In this approach, the integrity measure of the system is computed based only on the present measurement, without reference to the past. RAIM algorithms belonging to the second class are called in the literature filtering (or averaging) algorithms. These algorithms use all of the measurements acquired up to the moment of decision, as well as a priori information (if available) about the dynamics of the user. Based on the assumption that a fault can occur only in a single satellite at a given time, the snapshot approach is the one commonly used today for RAIM purposes.

One of the common RAIM algorithms is based on the parity space approach for failure detection and isolation (FDI).[5,6] In this approach, the measurement is mapped into the orthogonal complement of the range space of the observation matrix, called the parity space. The result of this transformation is the parity vector, which is used as a statistic for detecting and identifying the faults. An underlying assumption of RAIM algorithms (which is common to many FDI methods) is that a fault can occur in just one satellite at a time. Detecting a fault is done by comparing the norm of the parity vector to an externally predetermined threshold value. (If the norm is greater than the threshold value a fault is declared.) Identification of the faulty satellite is done by comparing the parity vector's direction to the directions of the columns of the transformation matrix. (The number of columns is as many as the number of satellites acquired.) The faulty satellite is the one whose characterizing column in the transformation matrix is closest in direction to the parity vector. Experience shows that this algorithm copes very well with detecting faults, with a negligible false alarm rate; however, its false identification rate might be, in some situations, unacceptable. The identification process requires a minimum of six satellites to be acquired. When working close to this constraint, with six or seven satellites only, there might exist a proximity of directions between a number of columns of the transformation matrix. In this case, if a fault has indeed occurred in one of the satellites, a false identification of the faulty satellite is possible due to measurement noise. Because the snapshot method works on the principle of removing the satellite identified as faulty from the solution, that is, the faulty satellite is not used for solving for the position and velocity, a situation

Presented as Paper 2003-5668 at the AIAA Guidance, Navigation, and Control Conference, Austin, TX, 11–14 August 2003; received 15 November 2003; revision received 23 March 2005; accepted for publication 7 April 2005.

*Professor, Department of Aerospace Engineering; yaakov.oshman@technion.ac.il. Associate Fellow AIAA.

†Research Engineer, Philadelphia Flight Control Laboratory, Department of Aerospace Engineering.

is possible where a healthy satellite is removed, while the faulty satellite is retained in the solution. When only a few satellites are acquired, removing a healthy satellite and retaining a faulty satellite in the navigation solution might result in positioning errors larger than those that would have been expected had all satellites (including the faulty one) been used for the solution. Moreover, because the spoofer chooses the location and time for generating the interference signal, it knows the geometry of the satellites in the area at the relevant time. Thus, the spoofer can compute the transformation matrix and optimize the spoofing effectiveness by choosing the satellite whose corresponding column is close in direction to other columns of the matrix. Clearly, then, in such a case the use of the snapshot algorithm might not be very effective. Note that this conclusion is true for the entire range of snapshot algorithms because it is possible to demonstrate their equivalence.[6]

The disadvantages of snapshot algorithms in coping with the problem of intentional interference with GPS operation gave rise to the hope that the filtering approach would provide a better solution to the disturbance problem because it uses more information than the snapshot approach. Da and Lin[7] present a method based on using a main Kalman filter, which processes all acquired measurements, and a bank of auxiliary filters processing subgroups of measurements. The detection process is based on testing the consistency of the results using the χ^2 test. No attempt is made to estimate the interference, but only to identify the faulty satellite to remove it from the solution. Thus, the method is similar in nature to snapshot RAIM algorithms because the navigation solution is obtained after making a binary decision on the health of each of the satellites and removing the faulty satellite. In Ref. 2, two independent algorithms for dealing with jamming and spoofing disturbances are presented. The spoofing problem is handled via a bank of Kalman filters, whereby the spoofing detection is performed via a χ^2 innovations test. The satellite identified as faulty is excluded, rendering this method as well similar in nature to snapshot RAIM algorithms. In Ref. 1, it is suggested to use a static multiple-model estimator to identify jamming and spoofing disturbances. Although White et al.[1] state that "an intelligent spoofer would place unique offsets on each of the satellite vehicles (SV) pseudorange measurements, producing a specific position offset desired by the spoofer," it is assumed that spoofing biases are inserted as either step or ramp offsets added uniformly to all GPS SV measurements. Obviously, this kind of disturbance is equivalent to an added clock bias, which can be handled quite effectively by the GPS receiver without resorting to special means and algorithms. Chen and Harigae[3] have recently suggested the use of the interacting multiple model (IMM) algorithm to identify jamming in a differential GPS/INS integrated system. Jamming is represented by an increased measurement noise, acting uniformly on all acquired channels, and the method presented in Ref. 3 aims at alleviating a jamming situation by identifying the true level of the measurement noise covariance out of three possible predefined values, corresponding to system states designated as "normal," "interference," and "jamming."

This paper introduces a method for making the GPS solution more robust in the presence of intentional spoofing by using the IMM filtering algorithm. Compared to snapshot RAIM algorithms, the adaptive algorithm presented herein offers a significant performance improvement, which results from its different mode of operation. Contrary to RAIM algorithms, the IMM-based approach is not based on binary decisions regarding the integrity of each of the acquired signals; instead, a probabilistic integrity measure is used, which facilitates the computation of the scheme's overall navigation solution based on all (properly weighted) available data. A simulation study is used to compare the performance of the proposed algorithm to that of the common snapshot RAIM algorithm in a wide range of scenarios.

The remainder of this paper is organized as follows. In the next section, a mathematical definition of the GPS navigation problem and the underlying assumptions are presented. A well-known snapshot RAIM algorithm, which serves here as a baseline to which the IMM-based algorithm is compared, is presented next. In the following section, the IMM algorithm is described and implemented in a form that best suits the problem under investigation. The results of an extensive simulation study that was performed to assess the performance of the IMM algorithm are then presented. Concluding remarks are offered in the final section.

II. GPS Navigation Problem

The basic measurement carried out by all GPS receivers is that of the time it takes the signal to cross the distance between the GPS satellite and the receiver. The errors in this measurement stem from nonsynchronization of the satellite clock with that of the receiver, as well as from delays in the signal as it passes through various parts of the atmosphere. Called pseudorange, the measured range is obtained by multiplying the measured time by the speed of light. For n acquired satellites, the pseudoranges are given by

$$\rho_i = r_i + b + v_i, \qquad i = 1, 2, \ldots, n \tag{1}$$

where ρ_i is the pseudorange corresponding to satellite i, r_i is the true range, b is the unknown bias of the receiver clock, in units of distance, and v_i is the measurement error due to atmospheric delays, which are not accounted for in the model. The true range can be computed as

$$r_i = \sqrt{\left(x - s_{i_x}\right)^2 + \left(y - s_{i_y}\right)^2 + \left(z - s_{i_z}\right)^2}, \qquad i = 1, 2, \ldots, n \tag{2}$$

where x, y, and z are the receiver's position coordinates and $\boldsymbol{s}_i \triangleq [s_{ix} \;\; s_{iy} \;\; s_{iz}]^T$ is the position vector of the ith satellite. Eq. (1) may be rewritten as

$$\boldsymbol{\rho} = \boldsymbol{\varphi}(\boldsymbol{s}_1, \boldsymbol{s}_2, \ldots, \boldsymbol{s}_n, \boldsymbol{\xi}) + \boldsymbol{v} \tag{3}$$

where $\boldsymbol{\varphi} = [\varphi_1 \;\; \varphi_2 \;\; \ldots \;\; \varphi_n]^T$ and $\varphi_i \triangleq r_i + b$, $\boldsymbol{\rho} \triangleq [\rho_1 \;\; \rho_2 \;\; \ldots \;\; \rho_n]^T$ is the vector of measured pseudoranges, $\boldsymbol{\xi} \triangleq [x \;\; y \;\; z \;\; b]^T$ is the vector of unknowns of the GPS navigation problem, and $\boldsymbol{v}$ is the measurement noise vector, commonly assumed to be a white, zero-mean, Gaussian distributed stationary sequence with covariance $\sigma_v^2 I_n$, where I_n is the n-dimensional identity matrix.

Linearization of Eq. (3) about a nominal value of the unknowns vector $\boldsymbol{\xi}^\star$ yields

$$\boldsymbol{y} = G\delta\boldsymbol{\xi} + \boldsymbol{v} \tag{4}$$

where

$$\boldsymbol{y} = \boldsymbol{\rho} - \boldsymbol{\varphi}(\boldsymbol{s}_1, \boldsymbol{s}_2, \ldots, \boldsymbol{s}_n, \boldsymbol{\xi}^\star) \tag{5a}$$

$$\delta\boldsymbol{\xi} = \boldsymbol{\xi} - \boldsymbol{\xi}^\star \tag{5b}$$

$$G = \left.\frac{\partial \boldsymbol{\varphi}(\boldsymbol{s}_1, \boldsymbol{s}_2, \ldots, \boldsymbol{s}_n, \boldsymbol{\xi})}{\partial \boldsymbol{\xi}}\right|_{\xi = \xi^\star}$$

$$= \left.\begin{bmatrix} \dfrac{x - s_{1_x}}{\rho_1 - b} & \dfrac{y - s_{1_y}}{\rho_1 - b} & \dfrac{z - s_{1_z}}{\rho_1 - b} & 1 \\ \dfrac{x - s_{2_x}}{\rho_2 - b} & \dfrac{y - s_{2_y}}{\rho_2 - b} & \dfrac{z - s_{2_z}}{\rho_2 - b} & 1 \\ \vdots & \vdots & \vdots & \vdots \\ \dfrac{x - s_{n_x}}{\rho_n - b} & \dfrac{y - s_{n_y}}{\rho_n - b} & \dfrac{z - s_{n_z}}{\rho_n - b} & 1 \end{bmatrix}\right|_{\xi = \xi^\star} \tag{5c}$$

Eq. (4) constitutes the basis for the well-known iterated least-squares (ILS) solution of the GPS navigation equations, as well as for all snapshot RAIM algorithms. As already noted, it is common to assume that $\boldsymbol{v}$, which describes the unmodeled measurement errors, can be characterized as a white or wideband noise. Obviously, if there is a deliberate interference or a malfunction in one or more of the satellites (or a multipath error), this assumption is no longer valid. In this case, the role of RAIM algorithms is to identify the satellite (or satellites) that are affected and to remove them from the solution.

To complete the description of the GPS navigation problem, it is assumed that the external disturbance (or malfunction) can appear in only one of the acquired satellites at a time. The extension of the algorithm presented in this paper to the multisatellite spoofing case is discussed in Sec. IV.B, Remark 4.

III. Snapshot RAIM Algorithm

The well-known and widely used parity space-based snapshot RAIM algorithm[5,6,8] serves in this work as a baseline algorithm to which the proposed filtering algorithm is compared. The algorithm comprises the following two stages.

A. Fault Detection

Let $\mathcal{H}_0$ denote the null hypothesis, that is, the hypothesis that all acquired satellites perform nominally. Let $\mathcal{H}_1$ denote the alternate hypothesis, that is, the hypothesis that there is a malfunction in one of the acquired satellites. The detection problem can be formulated as a statistical problem of deciding between the two hypotheses.

The first stage in the detection process consists of a check on the number of acquired satellites. Thus, to detect a malfunction, the number of acquired satellites, n, must satisfy the following condition:

$$n \geq 5 \tag{6}$$

The detection process is based on the parity vector $\boldsymbol{p}$, which is defined as a transformation of the measurement vector $\boldsymbol{y}$ into the null space of G^T (the orthogonal complement of the range space of G), which is termed the parity space. The parity vector is computed as

$$\boldsymbol{p} = P\boldsymbol{y}, \qquad \boldsymbol{p} \in \mathbb{R}^{n-4} \tag{7}$$

The matrix $P \in \mathbb{R}^{n-4,n}$ satisfies

$$P^T P = S \tag{8}$$

where

$$S \triangleq I - G(G^T G)^{-1} G^T \tag{9}$$

The matrix P can be computed via a QR decomposition of G, yielding P as the lowest $n-4$ rows of the matrix Q^T.

The decision regarding the existence of malfunction is made by examining the square of the norm of the parity vector. Thus,

$$\|\boldsymbol{p}\|^2 \underset{<}{\overset{\mathcal{H}_1}{\geq}} T_D \tag{10}$$
$$\mathcal{H}_0$$

where T_D is the decision threshold. T_D is computed offline and is a function of the prespecified false alarm probability P_{FA}, the variance of the measurement noise σ_v^2, and the number of redundant measurements, $n-4$. T_D can be computed from the equation[5]

$$P_{\text{FA}} = \Psi\left(T_D \big/ \sigma_v^2 \middle| n-4\right) \tag{11}$$

where $\Psi(\chi^2|r) \triangleq 1 - P(\chi^2|r)$ and $P(\chi^2|r)$ is the χ^2 cumulative probability distribution function with r degrees of freedom,

$$P(\chi^2|r) = \left[2^{r/2}\Gamma\left(\frac{r}{2}\right)\right]^{-1} \int_0^{\chi^2} t^{r/2-1} \exp\left(-\frac{t}{2}\right) \mathrm{d}t \tag{12}$$

When six satellites are observed, the threshold can be computed as[8]

$$T_D = 2\sigma_v^2 \, \ell n(1/P_{\text{FA}}) \tag{13}$$

When $\|\boldsymbol{p}\|$ is chosen as the test statistic, the threshold value is set to $\sqrt{T_D}$.

B. Fault Identification

For the purpose of fault identification, the number of acquired satellites must satisfy the following constraint:

$$n \geq 6 \tag{14}$$

Notice that, as could be expected, more satellites are needed to enable fault identification than the number of satellites required for fault detection. The identification process is based on the vector $\boldsymbol{f} \in \mathbb{R}^n$, computed as

$$\boldsymbol{f} = S\boldsymbol{y} \tag{15}$$

where $S \in \mathbb{R}^{n,n}$ is given by Eq. (9). Now compute

$$\alpha_i \triangleq f_i^2 \big/ S_{ii}, \qquad i = 1, 2, \ldots, n \tag{16}$$

where f_i is the ith component of $\boldsymbol{f}$ and S_{ii} is the ith diagonal entry of the matrix S. The faulty satellite, corresponding to the index i_f, is declared according to the maximum likelihood approach as[5]

$$i_f = \arg \max_{i=1,2,\ldots,n} \alpha_i \tag{17}$$

With the faulty satellite identified, it can now be removed from the set of acquired satellites, and the (ILS or filtering) navigation solution can be carried out using the remaining $n-1$ satellites.

Remark 1: If a snapshot RAIM algorithm is used and the position solution is obtained by means of the ILS algorithm, the decision concerning the affected satellite and the position solution are based solely on present measurements, without consideration of measurement history. Moreover, in this case the solution completely disregards the acceleration of the carrying platform, rendering it applicable to both static and dynamic platforms. This is a clear advantage of the snapshot approach, whose disadvantages were discussed earlier in this paper, because the use of a filtering method necessitates making assumptions regarding the dynamics of the carrying platform, which renders the solution case dependent and not general.

IV. IMM Navigation in the Presence of Spoofing

The IMM filter[9] assumes that at any point in time the system under consideration obeys one of a finite number of models (modes) and that it can switch between these modes in accordance with a known transition probability matrix. The approach is based on using a filter bank consisting of elemental filters, each tailored to one of the possible modes of the system, that is, n filters corresponding to n modes, or hypotheses on the behavior of the system. At the beginning of each filtering cycle, the IMM algorithm mixes the previous cycle's mode-conditioned estimates and covariances using mixing probabilities computed in the previous cycle. The mixed variables are then used to initialize the elemental filters, which process the measurements to derive the updated estimates, covariances, and mode likelihood functions. The likelihood functions then serve to compute the mode probabilities and the mixing probabilities for the next cycle, whereas the updated estimates and covariances serve to compute combined state estimate and covariance. These can be regarded as the outputs of the IMM scheme.

For completeness, the IMM is briefly described herein. The interested reader is referred to Ref. 10, Sec. 11.6, for complete details.

A. IMM Estimator

The IMM algorithm comprises four stages.

Interaction

For $i, j = 1, 2, \ldots, n$, assume that $M_j(k)$ is the jth system mode, corresponding to the jth hypothesis on the model of the system at time k. The known mode transition probability matrix, whose entries are defined as

$$p_{ij} \triangleq \text{Prob}[M_j(k) \mid M_i(k-1)] \tag{18}$$

allows to calculate the mixing probability as

$$\mu_{i|j}(k-1) \triangleq \text{Prob}\left[M_i(k-1)|M_j(k), \mathcal{Z}^{k-1}\right] = \frac{p_{ij}\mu_i(k-1)}{\sum_{i=1}^{n} p_{ij}\mu_i(k-1)} \tag{19}$$

where the mode probability is

$$\mu_j(k) \triangleq \text{Prob}\left[M_j \middle| \mathcal{Z}^k\right] \tag{20}$$

and $\mathcal{Z}^k$ denotes the measurement history up to time k. The mixed state and covariance matrix for the filter assuming the model $M_j(k)$, denoted by $\hat{\boldsymbol{x}}_0^j(k-1|k-1)$ and $P_0^j(k-1|k-1)$, respectively, are

$$\hat{\boldsymbol{x}}_0^j(k-1|k-1) = \sum_{i=1}^{n} \hat{\boldsymbol{x}}^i(k-1|k-1)\mu_{i|j}(k-1|k-1) \tag{21a}$$

$$\begin{aligned} P_0^j(k-1|k-1) = \sum_{i=1}^{n} \mu_{i|j}(k-1|k-1)\Big\{ & P^i(k-1|k-1) \\ & + \left[\hat{\boldsymbol{x}}^i(k-1|k-1) - \hat{\boldsymbol{x}}_0^j(k-1|k-1)\right] \\ & \times \left[\hat{\boldsymbol{x}}^i(k-1|k-1) - \hat{\boldsymbol{x}}_0^j(k-1|k-1)\right]^T \Big\} \end{aligned} \tag{21b}$$

Filtering

For $j = 1, 2, \ldots, n$, a bank of n Kalman filters is used to compute the state estimate $\hat{\boldsymbol{x}}^j(k|k)$ and estimation covariance matrix $P^j(k|k)$, starting from the estimate and covariance in Eqs. (21a) and (21b), respectively, and assuming model M_j for the transition from time $k-1$ to time k. The likelihood function corresponding to mode j can be computed using the innovations generated by the associated Kalman filter as

$$\begin{aligned} \Lambda_j(k) = p\left[\boldsymbol{z}(k)\middle|M_j, \mathcal{Z}^{k-1}\right] = 1\Big/\left\{(2\pi)^{n/2}[\det A_j(k)]^{\frac{1}{2}}\right\} \\ \times \exp\left\{-\tfrac{1}{2}\boldsymbol{r}_j^T(k)A_j^{-1}(k)\boldsymbol{r}_j(k)\right\} \end{aligned} \tag{22}$$

where $\boldsymbol{r}_j(k)$ and $A_j(k)$ are the innovations sequence and innovations covariance corresponding to mode j, respectively.

Mode Probabilities

Each mode probability $\mu_j(k)$, $j = 1, 2, \ldots, n$, is computed by

$$\mu_j(k) = \frac{p\left[\boldsymbol{z}(k)\middle|M_j, \mathcal{Z}^{k-1}\right]\text{Prob}\left[M_j\middle|\mathcal{Z}^{k-1}\right]}{p[\boldsymbol{z}(k)|\mathcal{Z}^{k-1}]} \tag{23}$$

Using $\Lambda_j(k)$, which is computed using the innovations process statistics as shown in Eq. (22), Eq. (23) can be rewritten as

$$\mu_j(k) = \frac{\Lambda_j(k)\sum_{i=1}^{n} p_{ij}\mu_i(k-1)}{\sum_{j=1}^{n}\Lambda_j(k)\sum_{i=1}^{n} p_{ij}\mu_i(k-1)} \tag{24}$$

Final Estimates

The mode probabilities, along with each filter's state estimate and estimation error covariance matrix are used to compute a new combined state estimate and covariance. These constitute the output of the IMM scheme,

$$\hat{\boldsymbol{x}}(k|k) = \sum_{j=1}^{n} \hat{\boldsymbol{x}}^j(k|k)\mu_j(k) \tag{25a}$$

$$\begin{aligned} P(k|k) = \sum_{j=1}^{n} \mu_j(k)\{P^j(k|k) + [\hat{\boldsymbol{x}}^j(k|k) - \hat{\boldsymbol{x}}(k|k)] \\ \times [\hat{\boldsymbol{x}}^j(k|k) - \hat{\boldsymbol{x}}(k|k)]^T\} \end{aligned} \tag{25b}$$

In the case under investigation in this paper, the IMM filter bank comprises a set of extended Kalman filters (EKFs), one per each hypothesis regarding the disturbance character. EKFs are used because of the nonlinearity of the measurement equation. These filters are briefly described next.

B. IMM Elemental Filters

Each EKF in the IMM filter bank is based on the following model.

Propagation Model

Assuming that the platform carrying the GPS receiver is not undergoing severe accelerations, the propagation model used in this work is based on Singer's kinematic model (see Ref. 11). The platform acceleration is modeled as a zero-mean random process with exponential autocorrelation. Let

$$\boldsymbol{\zeta} \triangleq [x \quad y \quad z \quad \dot{x} \quad \dot{y} \quad \dot{z} \quad \ddot{x} \quad \ddot{y} \quad \ddot{z}]^T \tag{26}$$

be the platform's state vector, then Singer's discrete-time model is

$$\boldsymbol{\zeta}_{k+1} = \Phi(T)\boldsymbol{\zeta}_k + \boldsymbol{w}_k \tag{27}$$

The transition matrix $\Phi(T)$ is given by

$$\Phi(T) = \left[\begin{array}{c|c|c} I_3 & TI_3 & (\alpha T - 1 + e^{-\alpha T})\big/\alpha^2 I_3 \\ \hline 0^{(3\times 3)} & I_3 & (1 - e^{-\alpha T})\big/\alpha I_3 \\ \hline 0^{(3\times 3)} & 0^{(3\times 3)} & e^{-\alpha T} I_3 \end{array}\right] \tag{28}$$

where T is the sampling period and $1/\alpha$ is the acceleration decorrelation time constant (selected to best characterize the platform at hand). The discrete-time process noise $\boldsymbol{w}_k$ has covariance $Q \in \mathbb{R}^9$, whose matrix elements are

$$\begin{aligned} Q_{11} = \left(\sigma_m^2\big/\alpha^4\right)(1 - e^{-2\alpha T} + 2\alpha T + 2\alpha^3 T^3/3 \\ - 2\alpha^2 T^2 - 4\alpha T e^{-\alpha T})I_3 \end{aligned} \tag{29a}$$

$$Q_{12} = \left(\sigma_m^2\big/\alpha^3\right)(e^{-2\alpha T} + 1 - 2e^{-\alpha T} + 2\alpha T e^{-\alpha T} - 2\alpha T + \alpha^2 T^2)I_3 \tag{29b}$$

$$Q_{13} = \left(\sigma_m^2\big/\alpha^2\right)(1 - e^{-2\alpha T} - 2\alpha T e^{-\alpha T})I_3 \tag{29c}$$

$$Q_{22} = \left(\sigma_m^2\big/\alpha^2\right)(4e^{-\alpha T} - 3 - e^{-2\alpha T} + 2\alpha T)I_3 \tag{29d}$$

$$Q_{23} = \left(\sigma_m^2\big/\alpha\right)(e^{-2\alpha T} + 1 - 2e^{-\alpha T})I_3 \tag{29e}$$

$$Q_{33} = \sigma_m^2(1 - e^{-2\alpha T})I_3 \tag{29f}$$

where σ_m^2 is the variance of the platform acceleration.

The entire filter's state is defined as

$$\boldsymbol{x} \triangleq \left[\boldsymbol{\zeta}^T \quad b \quad \tilde{b}^{(i)}\right]^T \tag{30}$$

where $\tilde{b}^{(i)}$ is the error in the range measurement of the ith satellite due to the sum of the effects of the clock bias and the external disturbance. The clock bias and the range error states are modeled in the filter as discrete-time random walk processes,

$$b_{k+1} = b_k + n_k \tag{31a}$$

$$\tilde{b}_{k+1}^{(i)} = \tilde{b}_k^{(i)} + \eta_k \tag{31b}$$

where $n_k \sim \mathcal{N}(0, \sigma_n^2)$ and $\eta_k \sim \mathcal{N}(0, \sigma_\eta^2)$.

Remark 2: Model (31) is, obviously, a crude model, and more elaborate ones could be used, for example, the model used in Ref. 12. However, as will be shown in the next section, this crude model satisfactorily copes with a very wide range of external disturbances, rendering the use of more sophisticated clock and disturbance models unnecessary.

Remark 3: If the GPS receiver is under high acceleration, it is possible to use one of the following two approaches. The first and the most widespread approach consists of integration of INS and GPS, as described in Ref. 13. In this approach, there is no need for any assumptions about the dynamics of the platform because the acceleration and angular velocity are measured directly by the inertial sensors, whereas the task of the GPS is to prevent the divergence

of the position, velocity and attitude estimates in the EKF solution. The disadvantage of this method is in the need for additional hardware [inertial measurement unit (IMU)]. A second approach suggests using the IMM estimation algorithm to choose between various feasible platform motion models.[14]

Measurement Model

Assuming that the jth satellite is faulty, the measurement model of Eq. (1) becomes

$$\rho_i = \begin{cases} \sqrt{(x-s_{i_x})^2+(y-s_{i_y})^2+(z-s_{i_z})^2}+b+v_i, \\ \qquad\qquad i=1,2,\ldots,n, \qquad i\neq j \\ \sqrt{(x-s_{i_x})^2+(y-s_{i_y})^2+(z-s_{i_z})^2}+\tilde{b}^{(j)}+v_i, \quad i=j \end{cases} \tag{32}$$

The EKF's observation matrix, obtained via linearization of the measurement equation (32), is

$$H = \left[\begin{array}{ccc|c|cc} \frac{x-s_{1_x}}{\rho_1-b} & \frac{y-s_{1_y}}{\rho_1-b} & \frac{z-s_{1_z}}{\rho_1-b} & & 1 & 0 \\ \frac{x-s_{2_x}}{\rho_2-b} & \frac{y-s_{2_y}}{\rho_2-b} & \frac{z-s_{2_z}}{\rho_2-b} & & 1 & 0 \\ \vdots & \vdots & \vdots & & \vdots & \vdots \\ \vdots & \vdots & \vdots & & \vdots & \vdots \\ \frac{x-s_{j_x}}{\rho_j-\tilde{b}^{(j)}} & \frac{y-s_{j_y}}{\rho_j-\tilde{b}^{(j)}} & \frac{z-s_{j_z}}{\rho_j-\tilde{b}^{(j)}} & 0^{n\times 6} & 0 & 1 \\ \vdots & \vdots & \vdots & & 1 & 0 \\ \vdots & \vdots & \vdots & & \vdots & \vdots \\ \frac{x-s_{n_x}}{\rho_n-b} & \frac{y-s_{n_y}}{\rho_n-b} & \frac{z-s_{n_z}}{\rho_n-b} & & 1 & 0 \end{array}\right]_{\xi=\xi^*} \tag{33}$$

where the single 0 in the 10th column and the single 1 in the 11th column appear in the jth row.

Remark 4: Following the customary assumption in RAIM algorithms, the IMM filter bank employed in this paper assumes the existence of a spoofing signal in one satellite, at most. In principle, the extension of this scheme to two spoofers (or more) is straightforward, provided, of course, that the system is observable: With n acquired satellites, no more than $n-4$ spoofing signals can be identified. When this condition is met, the required number of filters in an IMM bank designed for estimating m spoofers is $\binom{n}{m}$. For $n=6$ and $m=2$, this gives a bank of 15 elemental filters. This number might seem prohibitively large for various applications; however, note that 1) a filter bank designed for m spoofers covers all l-spoofer cases with $l<m$ (because each m-spoofer elemental filter can identify spoofing in any subset of its measurement channels, as will be demonstrated in the next section) and 2) the fact that the platform dynamics is common to all models should allow for massive parallelization to be used, reducing the overall computation time.

C. Discussion

Compared to the RAIM approach, the IMM algorithm is based on an entirely different mode of operation. Based on a dichotomy approach, the RAIM algorithm employs a binary decision procedure regarding each of the satellites involved in the navigation solution: By the comparison of the parity vector-based statistic against a preset threshold, the health state of each satellite is determined as either healthy or faulty, and, accordingly, this satellite is either retained in the solution or removed from it. Erroneous fault identification, which might happen in unfavorable satellite geometries, might lead to severe consequences in GPS applications: A healthy, correctly functioning satellite is removed from the solution, whereas the faulty satellite is retained in the navigation solution computations. Thus, the accuracy of the solution is reduced not only because of the faulty satellite, but also because of the removal of the functioning satellite.

In contradistinction to the detect, identify, and exclude methodology of the snapshot RAIM approach, the IMM adaptive filtering algorithm does not entail a hard, binary decision on the health state of the satellites involved in the solution. Rather, each satellite is assigned a probabilistic measure of its health (the posterior mode probability), and the solution is obtained by probabilistically weighting all available data (from all available satellites). Thus, the implied decision on the health status of each satellite is not a hard, binary one and is not achieved by comparing a statistic against an externally set threshold; rather, in the new method, the (implicit) decision is soft and is achieved by comparing each satellite's posterior probability against the probabilities assigned to the other satellites. As will be shown in the next section, this property yields a much improved identification capability and, at the same time, significantly reduces the effect of a wrong identification, should one occur, because no hard decisions are taken and no satellite is excluded (where wrong identification means, in the context of IMM methodology, wrong assignment of mode probabilities). Moreover, because the IMM algorithm estimates the disturbance (as opposed to the RAIM algorithm that tries to identify the disturbed satellite and exclude it), it can operate successfully with as few as five available satellites. (Recall that the minimum number of satellites required for RAIM identification is six.) Five available satellites operation will be shown next.

V. Simulation Study

To examine the performance of the new algorithm, an extensive simulation study was conducted. In this study, the IMM algorithm was compared to the RAIM algorithm, in the presence of a wide range of spoofing signals. This wide range was used to render the simulation conditions as general as possible. The number of satellites acquired throughout most of the simulation was six, the minimum required for fault identification using the RAIM algorithm. At the final stage of the simulation, this number was reduced to five, to examine the performance of the new method outside the RAIM operational envelope.

A. Simulation Description

In the simulated scenario, the platform performed a maneuver combined of east and north accelerations as shown in Fig. 1. The platform's initial position was latitude $= 32°46.4764'$ N and longitude $= 035°01.3434'$ E. The platform's altitude was 262 m. The maneuver started on 20 June 2002 at 12:05:00 Coordinated Universal Time and lasted for 1000 s. During this period, the following GPS satellites were observed under elevation mask of 10 deg: SV-01, SV-07, SV-11, SV-13, SV-19, and SV-20.

Throughout the simulation study, the IMM elemental filters were implemented with the parameter values shown in Table 1. The IMM

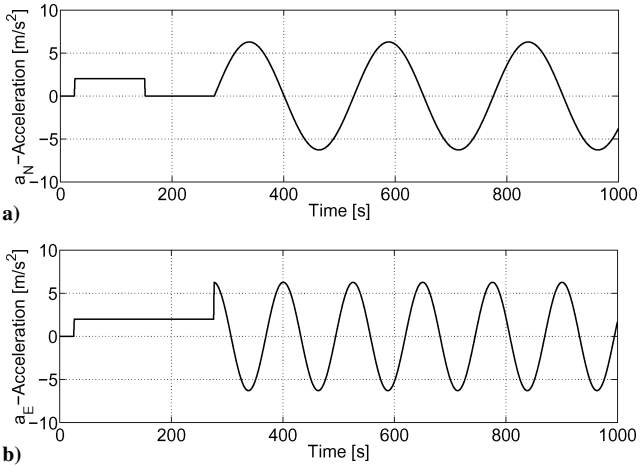

Fig. 1 Platform accelerations over 1000 s: a) north and b) east.

Table 1 Simulation parameters

Parameter	Value
σ_η	100 m
σ_n	70 m
σ_v	3 m
$1/\alpha$	100 s
T	1 s
σ_m	4.66 m/s^2

Table 2 Clock bias model parameters for various timing standards (Ref. 15)

Timing standard	h_0	h_{-1}	h_{-2}
Temperature-compensated crystal	2×10^{-19}	7×10^{-21}	2×10^{-20}
Ovenized crystal	8×10^{-20}	2×10^{-21}	4×10^{-23}
Rubidium	2×10^{-20}	7×10^{-24}	4×10^{-29}

transition probability matrix was

$$p_{ij}=\begin{cases}0.95+0.05/n, & i=j\\ 0.05/n, & i\neq j\end{cases} \tag{34}$$

where n is the number of acquired satellites.

The initial state estimate is obtained via the use of the ILS solution at time t_0. The initial estimation error covariance matrix was set in this study to

$$P_0=\text{diag}\{100^2, 100^2, 100^2, 1, 1, 1, 1, 1, 1, 100^2, 100^2\} \tag{35}$$

where the respective variances are in units of square meters, square meters per square seconds, and square meters/s^4.

The GPS clock model used in this study is the common model described in Ref. 15 (pp. 428–431). This model is based on the assumption that both the clock frequency and its phase behave like a random walk process over short-time intervals. Hence, the discrete-time clock bias model is given by

$$\boldsymbol{x}_k^c=\Phi^c(\Delta t)\boldsymbol{x}_{k-1}^c+\boldsymbol{w}_{k-1}^c \tag{36}$$

where

$$\boldsymbol{x}^c\triangleq\begin{bmatrix}b\\ \dot b\end{bmatrix},\qquad \Phi^c(\Delta t)=\begin{bmatrix}1 & \Delta t\\ 0 & 1\end{bmatrix} \tag{37}$$

$$Q^c\triangleq E[\boldsymbol{w}^c(\boldsymbol{w}^c)^T]=$$

$$\begin{bmatrix}(h_0/2)\Delta t+2h_{-1}\Delta t^2+\frac{2}{3}\pi^2h_{-2}\Delta t^3 & h_{-1}\Delta t+\pi^2h_{-2}\Delta t^2\\ h_{-1}\Delta t+\pi^2h_{-2}\Delta t^2 & h_0/(2\Delta t)+4h_{-1}+\frac{8}{3}\pi^2h_{-2}\Delta t\end{bmatrix} \tag{38}$$

Typical values for spectral density parameters associated with various types of clocks are given in Table 2. All clock types of Table 2 were tested in the simulations, without changing the filter's tuning parameters. In these simulations, the filter has exhibited no visible sensitivity to the clock model used. All simulations presented herein are based on the temperature-compensated crystal oscillator.

Remarks 5: Notice that the described clock model is used only in the "truth world" simulation and not in the IMM elemental filters. In these filters, the model used for the clock bias is the random walk model of Eq. (31a).

Finally, the RAIM algorithm's threshold value was computed using Eq. (13) for a required false alarm probability of $P_{\text{FA}}=3.33\times10^{-7}$. (This value was suggested in Ref. 16 and used in Ref. 8.)

B. Constant Spoofing

The performance of the RAIM algorithm is initially examined under the assumption that the measurements corresponding to SV-01 are contaminated by a constant 100-m bias. The GPS navigation solution is done via the common ILS algorithm.

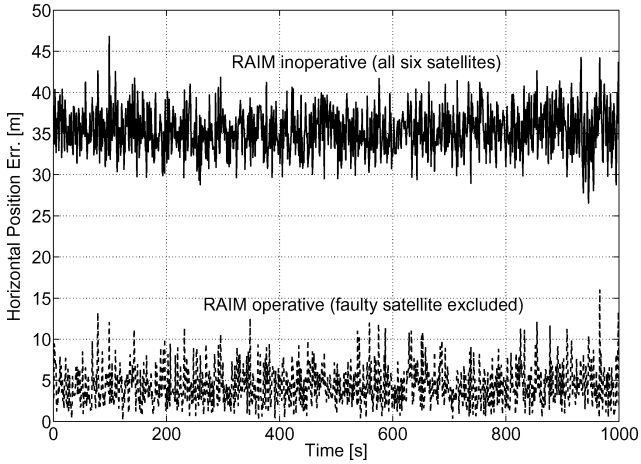

Fig. 2 Horizontal positioning error a 100-m bias in the range measurement of SV-01, with RAIM algorithm operative (dashed line) and inoperative (solid line). Geometry of a spoofed signal is favorable for identification by RAIM algorithm.

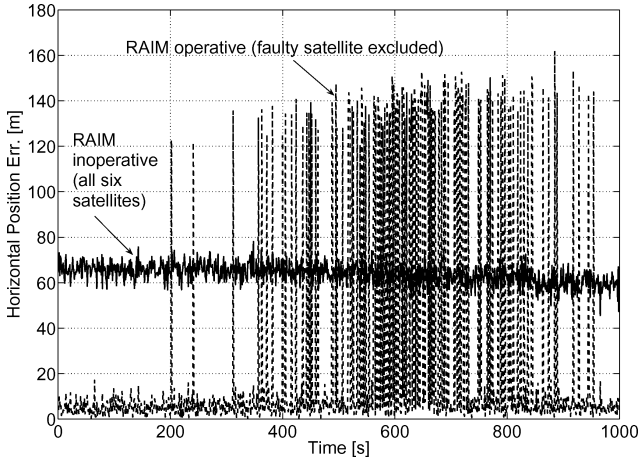

Fig. 3 Horizontal positioning error under a constant 100-m bias in the range measurement of SV-13, RAIM algorithm operative (dashed line) and inoperative (solid line) signal is not favorable for identification by RAIM algorithm.

Figure 2 shows the performance of the ILS algorithm with and without the RAIM algorithm. As can be observed, when the RAIM algorithm is inoperative, the horizontal positioning error reaches 35 m. The vertical positioning error (not shown for conciseness) behaves similarly and reaches about 60 m. Notice that this error is not constant in time, despite the fact that the pseudorange measurement bias is time invariant, because the geometry of the satellite constellation changes over time, which is known to affect the positioning error. When the RAIM algorithm is operative, both horizontal and vertical positioning errors are reduced significantly, indicating that the RAIM algorithm works flawlessly.

Suppose now that the bias of 100 m exists in the range measurement of the fourth acquired satellite, SV-13, instead of the first satellite. The estimation results in this case are shown in Fig. 3. Note that without the RAIM algorithm (solid line) the horizontal positioning error is about 65 m. The vertical positioning error (not shown for conciseness) is about 100 m. This solution is based on all six acquired satellites, including the faulty one.

When the RAIM algorithm is active (Fig. 3, dashed line), it always properly detects a fault. Hence, it identifies a satellite as faulty and removes it from the solution. Thus, the RAIM-based navigation solution is always based on just five satellites. Now, when the faulty satellite is correctly identified and removed, the solution is based on the five healthy satellites; this solution corresponds in Fig. 3 to the low-level error (about 5–10 m), which is the error that would have

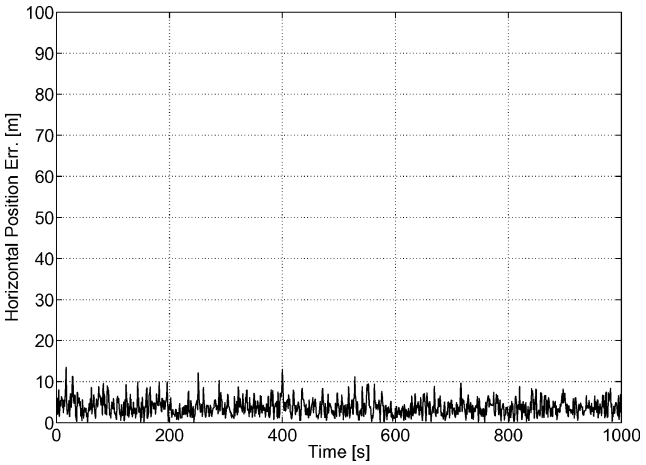

Fig. 4 Horizontal positioning error a constant 100-m bias in the range measurement of SV-13, IMM algorithm. Geometry of spoofed signal is not favorable for indentification by RAIM algorithm.

been obtained had there been no spoofing bias. On the other hand, the high-level error spikes (about 140 m) correspond to the many instances where the RAIM algorithm, due to the adverse geometry, incorrectly identifies a healthy satellite, namely, SV-20, as faulty. In these cases, the RAIM-based solution is based on four healthy satellites and one faulty satellite, all of which receive equal weighting in the solution. The navigation errors thus obtained are larger than those reached when the RAIM algorithm is not operative at all. This demonstrates the sensitivity of the RAIM algorithm to the geometry of the satellite constellation, when the number of acquired satellites is marginal, and emphasizes the potentially serious consequences of a wrong identification made by the RAIM algorithm.

Figure 4 shows the corresponding horizontal positioning error when the IMM algorithm is run. It can be seen that the 1-σ positioning error is no larger than 10 m. (The vertical error, not shown here, is similar.) When these results are compared to those obtained with the RAIM algorithm (Fig. 3), it can be concluded that the performance improvement obtained via using the IMM algorithm is about one order of magnitude. As earlier explained, unlike the RAIM algorithm, the IMM algorithm does not exclude any satellite from its navigation solution, which is, thus, based on all six satellites. Instead, the IMM algorithm estimates the spoofing signal and assigns proper probabilistic weight to the particular (spoofed) satellite, which is then taken into account along with all healthy satellites.

C. Periodically Switching Harmonic-Amplitude Spoofing

In reality, the spoofing disturbance can be of any kind and no a priori knowledge as to its character can be safely assumed. Thus, the performance of the algorithm was also examined in the presence of time-varying errors of an unknown model. To this end, the sinusoidal range measurement error shown in Fig. 5a was simulated. Moreover, to simulate a smart spoofer, the range measurement error was assigned to four of the six acquired satellites in the following manner, unknown to the GPS receiver: In the first 250 s, the faulty satellite was SV-01; between 250 and 500 s, the faulty satellite was SV-13; between 500 and 750 s, SV-07 was faulty; and between 750 and 1000 s, the fault was in SV-20. In each of these 250-s time intervals, the appropriate part of the sinusoidal range measurement error (Fig. 5a) was assigned to the corresponding satellite. Notice, that only one satellite (out of the six acquired) was faulty at all times, but the fault switched among the first, fourth, second, and sixth acquired satellites.

Figure 5a, which shows the true spoofing signal and its estimate, demonstrates that the IMM algorithm copes very well with this problematic scenario, which substantiates the random walk modeling of the error in the elemental IMM filters. The a posteriori mode probabilities obtained via the IMM algorithm are shown in Fig. 5b. Observe that the algorithm indeed correctly identifies the faulty satellite at nearly all times.

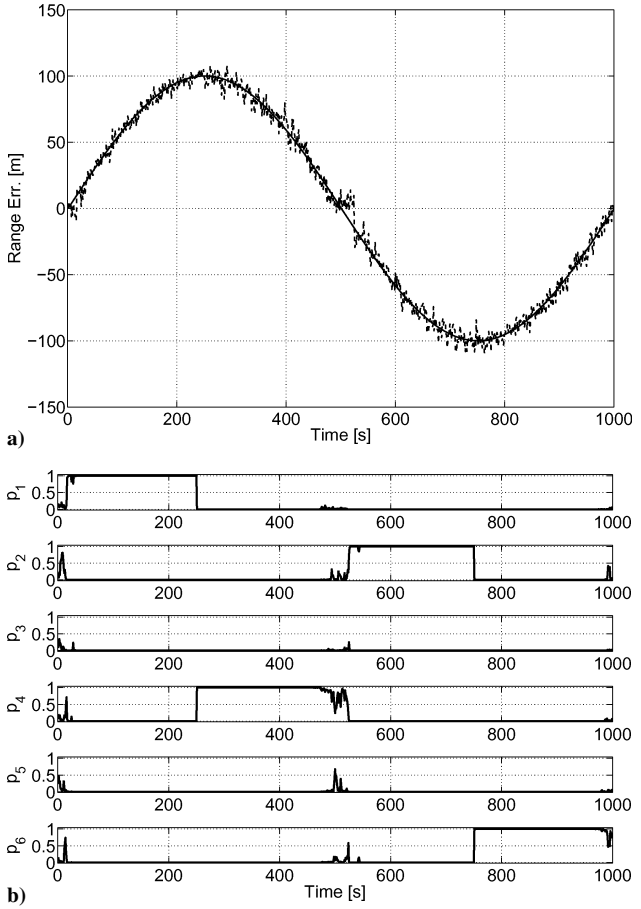

Fig. 5 Estimation performance of the IMM algorithm, periodic spoofing: a) spoofing signal: ——, true and – – –, estimated and b) mode probabilities.

The horizontal positioning errors with both IMM and RAIM algorithms in the presence of a periodic spoofing signal are compared in Fig. 6. (For conciseness, the vertical positioning error, which exhibited identical behavior, is not shown). The results are not significantly different than those obtained in the constant spoofing case. Whereas the IMM-based algorithm copes well with the presence of the spoofing signal, yielding positioning errors smaller than 10 m, the RAIM algorithm does not correctly identify the fault over a significant part of the estimation interval, generating positioning errors of up to 80 m when it is operative.

D. Randomly Switching Random-Amplitude Spoofing

The performance of the IMM algorithm was next examined in a scenario where the disturbance signal randomly switches among all acquired satellites at every measurement. The malfunctioning satellite was uniformly randomly selected from all observed satellites. The magnitude of the external disturbance was also randomly assigned at each measurement epoch, by sampling from a normal distribution with zero mean and variance of 100^2 m^2.

Figure 7 shows the horizontal positioning error of both methods under random spoofing. (Again, the vertical positioning error, which exhibited identical behavior, is not shown for conciseness.) The IMM algorithm copes well with the type of spoofing employed, and the positioning errors in this case are not significantly different than those obtained with a constant bias. In comparison, the snapshot RAIM algorithm exhibits errors larger than 100 m at times.

E. No Spoofing

The IMM filter introduced herein is not typical in that it does not include in its bank a filter matched to the null hypothesis, which is that no spoofing is active, that is, that all satellites are healthy. Thus, it might seem as if this scheme is not set to cope with a nominal,

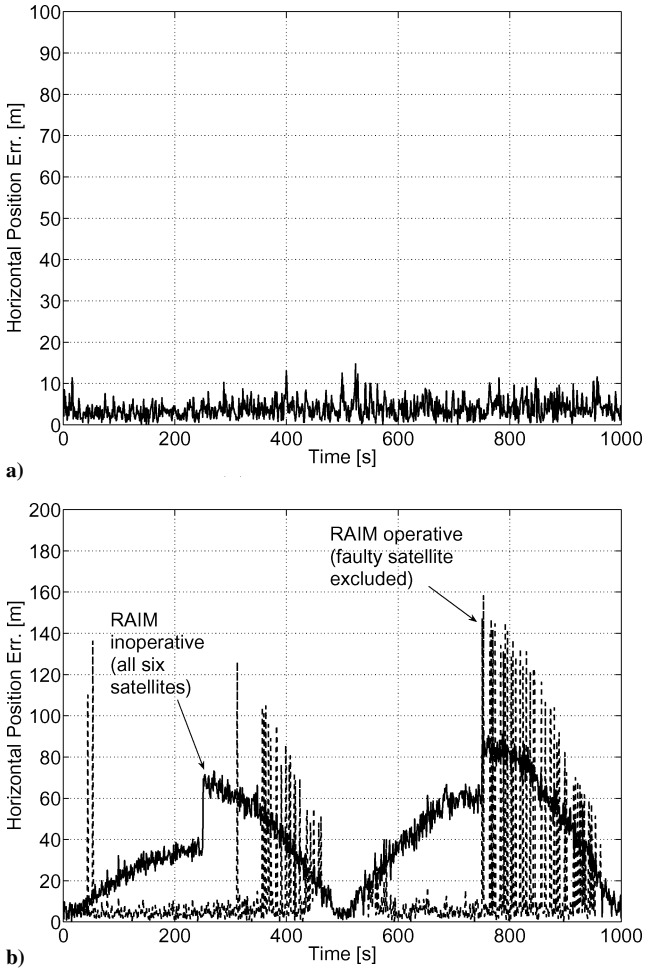

Fig. 6 Horizontal positioning error under periodic spoofing with a) IMM algorithm and b) RAIM algorithm: – – –, operative and b) ——, inoperative.

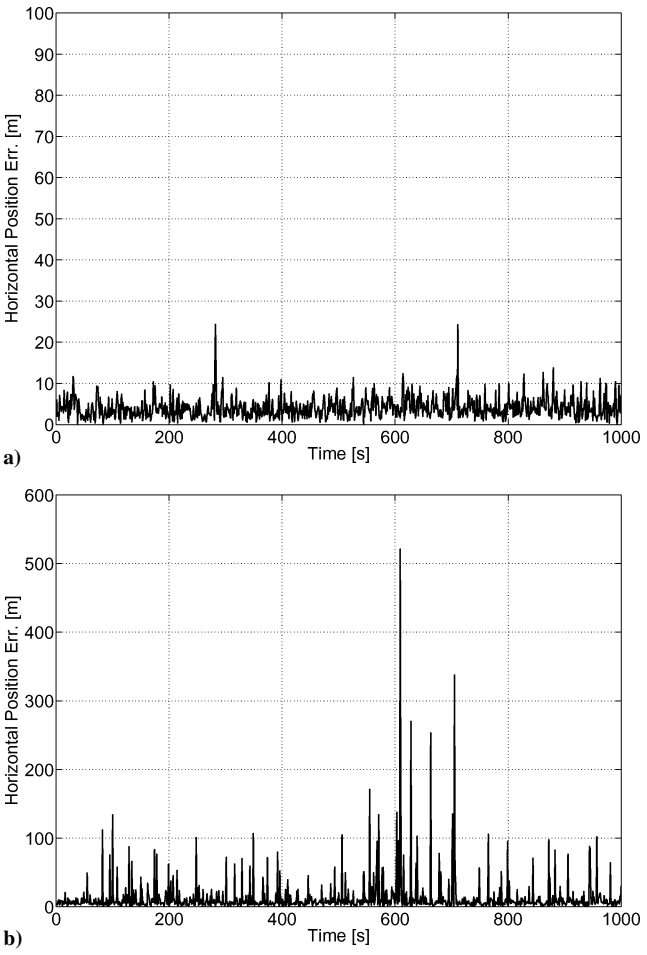

Fig. 7 Horizontal positioning error under random spoofing a) with IMM and b) RAIM algorithms.

disturbance-free scenario. To demonstrate that this is not the case, a simulation is performed for the scenario where a random disturbance (identical to the one considered in the preceding subsection) is activated only after 500 s of disturbance-free operation.

Figure 8 shows the estimation performance of the IMM filter in this case. It can be clearly seen that there is no noticeable difference in the filter's performance before and after the disturbance is started. This can be explained by noting that no-spoofing (zero bias) is just a special case of the general random bias case. Hence, when there is no bias, any of the IMM elemental filters can estimate the (zero) bias equally well. Figure 8b shows the mode probability time histories obtained using the IMM in this case. Because all elemental filters can serve to estimate the zero bias, the mode probabilities switch in a random fashion between the modes (depending on the current measurement noise values of all pseudoranges). This, however, does not affect the total performance of the IMM filter, as can be seen from Fig. 9, which shows the horizontal positioning error obtained using the IMM. Clearly, this error is not different than the errors obtained in preceding cases, for example, constant bias. The conclusion from this analysis is that, indeed, no special elemental filter is needed for the nominal (no bias) case.

F. Five Satellites

In all of the preceding tested scenarios, the number of satellites acquired was six. This number was selected because it is the minimal number of satellites required for using RAIM algorithms. Indeed, as earlier simulations show, the performance of RAIM algorithms when the number of acquired satellites is six can be quite poor compared to the performance of IMM-based detection and identification.

Because the IMM-based algorithm presented in this paper works quite differently than RAIM algorithms, it is conceivable that it does not have to obey the six-satellite threshold; in fact, because the IMM filter works by estimating the disturbance (unlike RAIM algorithms), it is plausible that only five satellites will suffice for its operation because, basically, the number of state variables it estimates is five: three position components, clock bias, and the external spoofing disturbance.

To verify that, indeed, the IMM algorithm can cope with a reduced number of acquired satellites, the elevation mask was increased to 13 deg (from the 10-deg mask used in the earlier simulations). In this case, the GPS receiver acquires just the SV-01, SV-11, SV-13, SV-19, and SV-20 satellites. (SV-07 is under the elevation mask and, hence, it is not acquired.) All other simulation parameters remain as in the preceding cases.

To demonstrate the performance of the algorithm with five satellites only, a combined spoofing signal was tested, which consists, essentially, of a time concatenation of all earlier tested disturbance signals (Fig. 10a). Thus, the spoofing signal is built of a piecewise-constant switching signal with random amplitude (applied to satellites SV-01, SV-11, SV-20, SV-19, and SV-13, in this order, between 0 and 500 s), a periodic signal applied to SV-11 (between 500 and 750 s), and a random switching signal with random amplitude (between 750 and 1000 s). Notice that the first 500 s also include disturbance-free periods. Figure 10 demonstrates the performance of the algorithm in this case. Observe that the algorithm performs adequately, correctly identifies the disturbed satellite and estimates the disturbance at all times, and, thus, correctly estimates the position.

When the performance of the algorithm is compared to the earlier cases (where six satellites were acquired), it becomes clear (as could be expected) that the estimation performance degrades with the reduction in the number of acquired satellites. However,

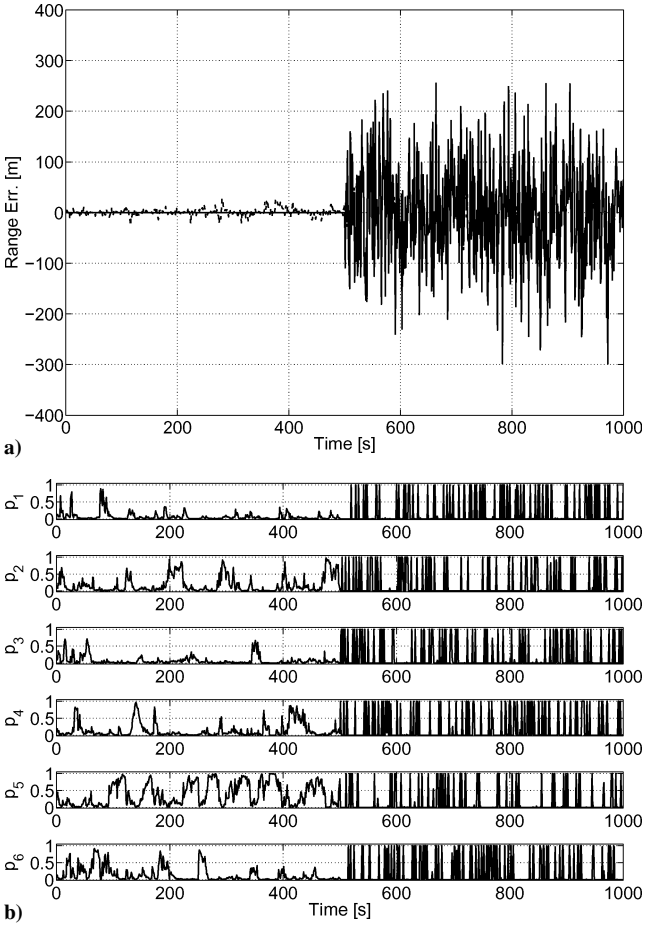

Fig. 8 Estimation performance of the IMM algorithm with random spoofing starting at t = 500 s: a) spoofing signal: solid line, true and dashed line, estimated and b) mode probabilities.

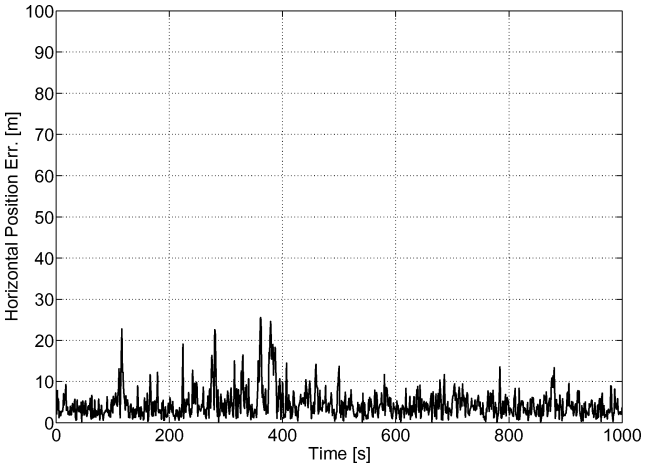

Fig. 9 Horizontal positioning error, IMM algorithm, with random spoofing starting at t = 500 s.

the degradation observed when reducing the number of satellites from 6 to 5 is minimal.

Note that the present IMM filter bank that was designed to handle a single spoofing signal was also tested in the case of two active spoofers (see Remark 4). In this test, constant, 100-m bias spoofing signals were applied to all possible 15 two-satellite combinations from the six acquired satellites. As could be expected, the filter could not handle this situation, and (nondiverging) positioning errors of hundreds of meters were observed in all cases.

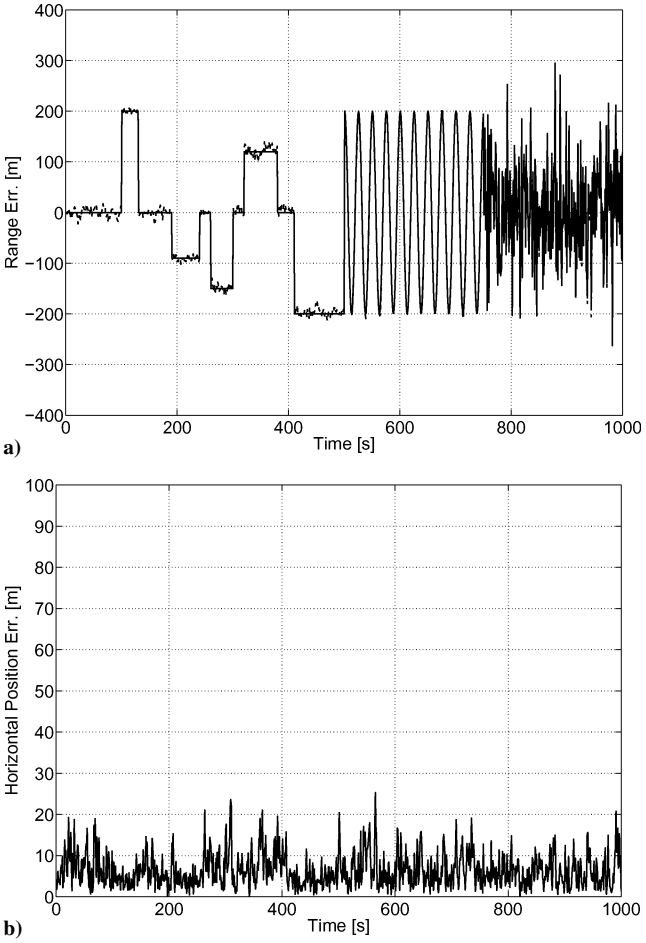

Fig. 10 IMM estimation performance in presence of combined spoofing, with only five satellites acquired: a) spoofing signal: solid line, true and dashed line, estimated and b) horizontal positioning error.

VI. Conclusions

A new concept, leading to improved immunity against spoofing disturbances in GPS applications, has been presented. The concept, which may be considered as a viable complementary or alternative method to the traditional snapshot RAIM algorithm, is based on the use of an IMM adaptive estimator that detects the existence of an external disturbance and implicitly identifies it by means of computing the posterior mode probabilities of various error models. The common case of signal jamming is not addressed in this work; this type of disturbance is usually adequately dealt with by state-of-the-art RAIM algorithms and by signal conditioning methods employed by the receiver within its signal processing circuitry.

With the use of an extensive computer simulation study, it has been demonstrated that the common RAIM algorithm of the snapshot type is sensitive to satellite constellation geometry, when working with a minimal number of satellites, and that there are geometries where it might not correctly identify the faulty satellite. The RAIM algorithm works by reaching a binary decision regarding the health of each of the satellites involved in the navigation solution. According to this decision, each satellite is either retained in the solution (if it is declared healthy) or removed from it (if it is declared faulty). When a nominally functioning satellite is excluded from the navigation solution due to an erroneous fault identification, this might lead to large navigation errors because, in addition, the true faulty satellite is retained.

Compared to the detect, identify, and exclude approach of snapshot RAIM algorithms, the adaptive filtering algorithm presented works by estimating the disturbance signal while retaining all acquired satellites in the navigation solution. Each satellite is assigned a probabilistic measure of its health, and the solution is obtained by probabilistically weighting all available data. Thus, the implied

decision on the health status of each satellite is not a hard, binary one and is not achieved by comparing a statistic against an externally set threshold. Rather, in the new method the (implicit) decision is soft and is achieved by comparing each satellite's posterior probability against the probabilities assigned to the other satellites. This yields an improved identification capability and enables an extended operational envelope.

An extensive simulation study is presented that demonstrates the accuracy and robustness of the new method with respect to a wide spectrum of disturbance signals. In addition, the study shows that the new method enables an expansion of the operational envelope of conventional RAIM algorithms (which are constrained to working with at least six acquired satellites) because it can properly function with just five satellites, with a negligible performance degradation. The proposed algorithm can be extended to handle spoofing in more than one satellite, subject to obvious observability constraints. This extension is a topic of current research.

Acknowledgments

This research was supported by the Robert and Mildred Rosenthal Aerospace Engineering Fund and by the "Devorah" Fund of Technion—Israel Institute of Technology.

References

[1]White, N. A., Maybeck, P. S., and DeVilbiss, S. L., "Detection of Interference/Jamming and Spoofing in DGPS-Aided Inertial System," *IEEE Transactions on Aerospace and Electronic Systems*, Vol. 34, No. 4, 1998, pp. 1208–1217.

[2]Vanek, B. J., Maybeck, P. S., and Raquet, J. F., "GPS Signal Offset Detection and Noise Strength Estimation in Parallel Kalman Filter Algorithm," *Proceedings of the 12th International Technical Meeting of the Satellite Division of the Institute of Navigation (ION GPS-99)*, Inst. of Navigation, Alexandria, VA, 1999, pp. 2243–2252.

[3]Chen, G., and Harigae, M., "IMM Based Jamming Detection in a DGPS-Aided Inertial System," AIAA Paper 2001-1830, April 2001.

[4]Kalafus, R. M., "Receiver Autonomous Integrity Monitoring of GPS," Technical Rept., U.S. Dept. of Transportation, Transportation System Center, Project Memorandum DOT-TSC-FAA-FA36-1, Cambridge, MA, June 1987.

[5]Sturza, M. A., "Navigation System Integrity Monitoring Using Redundant Measurements," *NAVIGATION, Journal of the Institute of Navigation*, Vol. 35, No. 4, 1988–1989, pp. 483–501.

[6]Brown, R. G., "A Baseline RAIM Scheme and a Note on the Equivalence of Three RAIM Methods," *NAVIGATION, Journal of the Institute of Navigation*, Vol. 39, No. 3, 1992, pp. 301–316.

[7]Da, R., and Lin, C. F., "New Failure Detection Approach and its Application to GPS Autonomous Integrity Monitoring," *IEEE Transactions on Aerospace and Electronic Systems*, Vol. 31, No. 1, 1995, pp. 499–506.

[8]Brown, R. G., and Chin, G. Y., "GPS RAIM: Calculation of Threshold and Protection Radius Using Chi-Square Method—A Geometric Approach," *RAIM: Requirements, Algorithms and Performance*, Vol. 5, Global Positioning System: Papers Published in *NAVIGATION*, Inst. of Navigation, Washington, DC, 1998, pp. 155–178.

[9]Blom, H. A. P., and Bar-Shalom, Y., "The Interacting Multiple Model Algorithm for Systems with Markovian Switching Coefficients," *IEEE Transactions on Automatic Control*, Vol. 33, No. 8, 1988, pp. 780–783.

[10]Bar-Shalom, Y., Rong-Li, X., and Kirubarajan, T., *Estimation with Applications to Tracking and Navigation*, Wiley, New York, 2001, Sec. 11.6.

[11]Bar-Shalom, Y., and Fortmann, T. E., *Tracking and Data Association*, Academic Press, San Diego, CA, 1988, Sec. 4.5.

[12]Axelrad, P., and Brown, R. G., "GPS Navigation Algorithms," *Global Positioning System: Theory and Applications*, edited by B. W. Parkinson and J. J. Spiker Jr., Vol. 163, Progress in Astronautics and Aeronautics, AIAA, Reston, VA, 1996, pp. 409–433.

[13]Farrell, J. A., and Barth, M., *The Global Positioning System and Inertial Navigation*, McGraw–Hill, New York, 1999, pp. 246–250.

[14]Lin, X., Kirubarajan, T., Bar-Shalom, Y., and Li, X. R., "Enhanced Accuracy GPS Navigation Using the Interacting Multiple Model Estimator," *Proceedings of IEEE Aerospace Conference*, IEEE, Piscataway, NJ, 2001, pp. 1911–1923.

[15]Brown, R. G., and Hwang, P. Y. C., *Introduction to Random Signals and Applied Kalman Filtering*, Wiley, New York, 1997, pp. 428–431.

[16]Lee, Y., Van Dyke, K., DeCleene, B., Studenny, J., and Beckmann, M., "Summary of RTCA SC-159 GPS Integrity Working Group Activities," *Navigation: Journal of The Institute of Navigation*, Vol. 43, No. 3, 1996, pp. 307–338.